# Dynamic State Estimation for Virtual Synchronous Generator: A Comparative Study of EKF and UKF

Zixiang Ming, Yongli Zhu
Sun Yat-sen University, Guangzhou, China (mingzx@mail2.sysu.edu.cn, yzhu16@alum.utk.edu)

***Abstract*—This paper conducts a comparative study on the application of the Extended Kalman Filter (EKF) and Unscented Kalman Filter (UKF) in dynamic state estimation for a virtual synchronous generator (VSG). Simulations are carried out in Simulink for two cases (single-machine infinite-bus system and three-machine nine-bus system). Results show that in both undisturbed and disturbed situations, the mean frequency errors of the EKF and UKF are all at the scale of $10^{-4}$ Hz, the mean rotor angle errors are all at the scale of $10^{-1}$ rad, and the algorithm execution time costs are less than 0.4 seconds.**

***Index Terms*—dynamic state estimation, EKF, UKF, virtual synchronous generator.**

## I. Introduction

The transition to renewable energy has rapidly replaced traditional synchronous generators with inverter-based resources (IBRs), resulting in a decline in system inertia and posing challenges to grid stability. The virtual synchronous generator (VSG) has emerged as a promising control solution, addressing this issue by endowing IBRs with similar inertia response and damping characteristics to those of traditional synchronous motors. The core of VSG control lies in the accurate estimation of internal dynamic states (primarily rotor angle and frequency). Therefore, real-time and precise dynamic state estimation is of great significance, where the Extended Kalman Filter (EKF) and Unscented Kalman Filter (UKF) methods are two mainstream approaches used for dynamic state estimation.

In the field of dynamic state estimation (DSE), previous studies have explored various methods. In [1], Zhao et al. propose a general constrained robust dynamic state estimation framework based on the UKF method, and its validity has been verified on the IEEE 39-node system. In [2], Kotha et al. propose a hybrid whale-tunicate optimized UKF (HW-TO-UKF) method to tune UKF scaling parameters, addressing the slow convergence and semi-definiteness issues of conventional UKF for DSE. In [3], Wang et al. propose a fault-tolerant extended Kalman filter framework that incorporates a discrete distribution model to characterize the data loss mechanism, with simulations demonstrating its resilience and robustness in handling incomplete measurements.

Furthermore, there have also been studies conducted on VSG. In [4], Zhang et al. propose an improved VSG voltage and frequency regulation control strategy based on a small-signal model to address insufficient voltage and frequency support in power systems with large-scale IBRs. In [5], Zhang et al. introduce secondary frequency control to restore nominal frequency after load fluctuations and a virtual power-based synchronization strategy for smooth grid connection. In [6], Tahir et al. propose a modified VSG control strategy featuring a pre-synchronization process with voltage/frequency compensation signals, which enables seamless off-grid to on-grid switching, and improves frequency transient response and power stability during mode transitions.

This paper contributes to: 1) present a comparative study between EKF and UKF in dynamic state estimation for VSG in terms of the estimation accuracy and computational efficiency, 2) validate the two methods in both single-machine and multi-machine power system test cases, and 3) validate the two methods in both steady-state and disturbed situations.

## II. Problem Statement

VSG consists of two key internal states, namely the rotor angle $\theta$ and the rotor angular velocity $\omega$. The relationship between the rotor angular velocity $\omega$ and the frequency $f_n$ is $\omega = 2\pi f$. By conducting real-time filtering and tracking of these two quantities, the operational status of the VSG can be identified timely manner. In this study, the state variables of the Kalman filtering method are $X = [\theta, \omega]$. The Kalman filter inputs the state estimate $X_{k-1}$ from the previous moment into the predefined state equation $f(\cdot)$ to predict the next estimate, and then corrects this estimate via the measurement and observation equation $h(\cdot)$. The measurement variables in this study include the following:

$P_{ref}, Q_{ref}$ – The reference value of active and reactive power output of VSG;
$P_e, Q_e$ – The actual active and reactive power output of VSG;
$V_{ref}$ – The rated voltage of VSG;
$V$ – The actual operating voltage of VSG;
$\theta_{grid}$ – Phase of the grid voltage;

In fact, $P_{ref}$, $Q_{ref}$ and $V_{ref}$ are artificially defined control quantities, while $P_e$, $Q_e$ can be obtained by measuring the three-phase voltages $V_{abc}$ and three-phase currents $I_{abc}$ on the main circuit. First, the three-phase phasors are converted to the dq-rotating coordinate system to obtain $[V_d, V_q]^{\mathrm{T}}$ and $[I_d, I_q]^{\mathrm{T}}$, and then the following formulae are applied:

$$\begin{aligned} P_{ref} &= \frac{3}{2}(V_d I_d + V_q I_q) \\ Q_{ref} &= \frac{3}{2}(V_q I_d - V_d I_q) \end{aligned} \tag{1}$$

In this study, the MAE (mean absolute error) between the predicted state sequence and the actual value sequence will

979-8-3315-8138-1

be compared, and the execution time of the EKF and UKF algorithms will be investigated.

## III. Dynamic State Estimation for VSG via the Kalman Filtering Methods

This section will elaborate on the framework of the VSG dynamic state estimation proposed in this paper. A dynamic simulation model of the VSG is built in MATLAB/Simulink. Then, the formula of the two state estimators (EKF, UKF) and their advantages in this problem are stated.

### *A. Dynamic Modeling for VSG*

The dynamic modeling of virtual synchronous generators is the basis of state estimation. Its core idea is to simulate the rotor motion characteristics of synchronous generators, enabling power electronic converters to possess the frequency support and voltage regulation functions of synchronous generators.

When selecting state variables, consideration is given to observability and physical significance. The rotor power angle $\theta$ (unit: radian, rad) and rotor angular frequency $\omega$ (unit: rad/s) of the VSG are taken as the state variables of the system. The power angle $\theta$ reflects the relative phase relationship between the electromotive force between the VSG and the (remaining grid, directly determining the transmission characteristics of active power. The angular frequency $\omega$ reflects the frequency dynamic characteristics of the system. These two state variables constitute the state vector $x = [\theta, \omega]^{\mathrm{T}}$ in this paper, which is used to describe the dynamic behavior of the VSG.

Based on the classical swing equation of the synchronous generator, a continuous-time nonlinear state space model is established for the VSG as follows:

$$\frac{d}{dt}\begin{bmatrix}\theta \\ \omega\end{bmatrix} = \begin{bmatrix}\omega \\ \frac{1}{J}\left(\frac{P_{ref}-P_e}{\omega} - (k_f + D)(\omega - \omega_n)\right)\end{bmatrix} \quad (2)$$

where, $J$ is the virtual moment of inertia, which determines the response speed of the system to power disturbances; $kf$ and $D$ are damping coefficients that jointly affect the oscillation attenuation characteristics of the system. $P_{ref}$ is the reference value of active power and is input as a control parameter; $P_e$ is the actual output active power, which is a measurement of the system; $\omega_n = 2\pi f_n$ is the nominal angular frequency (e.g., $f_n = 60$Hz).

The observation equation is the key link that connects the state variables with the measurable output. In the VSG system, the active power output $P_e$ is selected as the observation variable. In Simulink, the modeling of the main circuit of this system is shown in Fig. 1. The converter on the left is controlled by the relevant algorithms of VSG.

According to the theory of power system analysis, $P_e$ satisfies the following expression:

$$P_e = \frac{E \cdot V}{X_{\text{total}}}\sin(\theta - \theta_{\text{grid}}) \quad (3)$$

where, $E$ is the internal electric potential of VSG, $V$ is the grid voltage, $X_{\text{total}}$ is the total reactance, and $\theta_{\text{grid}}$ is the phase

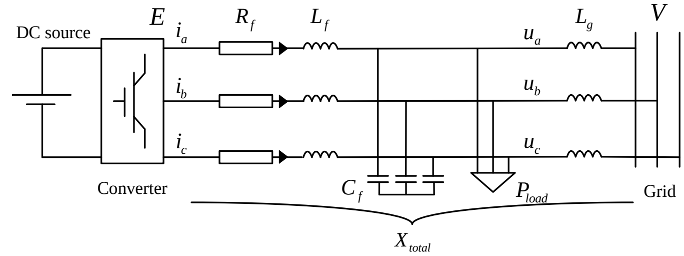


Fig. 1. The main circuit of VSG

of the grid voltage. In the actual system, the internal electric potential $E$ is not constant but is dynamically adjusted by the voltage control loop of the VSG. This paper uses an integral control-based voltage regulator for $E$:

$$E = E_0 + \int \left[k_p\left(V_{ref} - V\right) + k_i\left(Q_{ref} - Q\right)\right] dt \quad (4)$$

where, $V_{ref}$ and $Q_{ref}$ represent the reference values for voltage and reactive power, respectively, $Q$ represents the reactive power output of VSG, while $k_p$ and $k_i$ are control parameters. This control strategy enables the VSG to automatically adjust the internal electric potential to maintain the stability of the terminal voltage and provide reactive power support.

Finally, a typical control (transfer function) block diagram of the VSG system is shown in Fig. 2. It corresponds to the VSG dynamic modeling in Eq. (2), Eq. (4) and uses a dual-loop control to generate PWM signals for the DC-AC inverter.

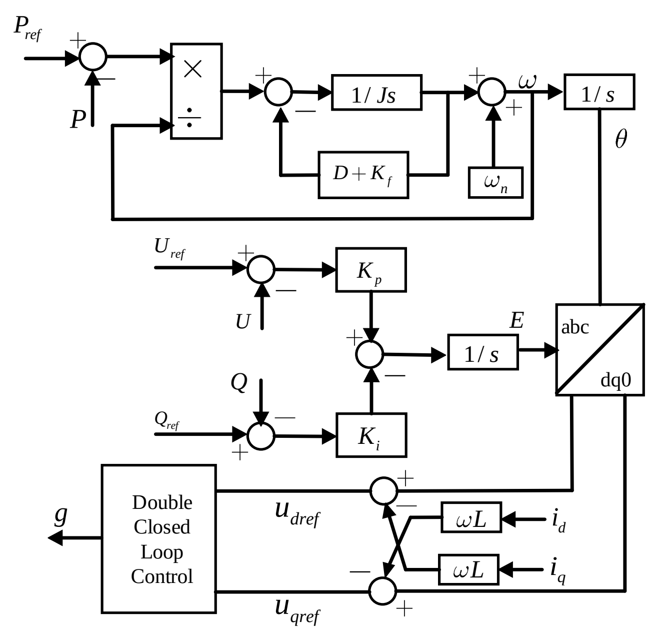


Fig. 2. A typical control block diagram of the VSG system

### *B. Dynamic State Estimation by Extended Kalman Filter*

*1) The basic steps of EKF:* EKF achieves state estimation by recursively performing the prediction and update steps. The

979-8-3315-8138-1

prediction step uses the system dynamic model to predict the state at the next time step; the update step refines the prediction using the latest observation. Its procedure is listed below:

$$\hat{\mathbf{x}}_k^- = f\left(\hat{\mathbf{x}}_{k-1}^+, \mathbf{u}_{k-1}\right) \tag{5}$$
$$\mathbf{P}_k^- = \mathbf{F}_{k-1}\mathbf{P}_{k-1}^+\mathbf{F}_{k-1}^T + \mathbf{Q} \tag{6}$$
$$\mathbf{K}_k = \mathbf{P}_k^-\mathbf{H}_k^T(\mathbf{H}_k\mathbf{P}_k^-\mathbf{H}_k^T + \mathbf{R})^{-1} \tag{7}$$
$$\hat{\mathbf{x}}_k^+ = \hat{\mathbf{x}}_k^- + \mathbf{K}_k\left(\mathbf{z}_k - h\left(\hat{\mathbf{x}}_k^-\right)\right) \tag{8}$$
$$\mathbf{P}_k^+ = \left(\mathbf{I} - \mathbf{K}_k\mathbf{H}_k\right)\mathbf{P}_k^- \tag{9}$$

where, $f(\cdot)$ is the nonlinear state transition function. $\mathbf{P}$ is the error covariance matrix. $\mathbf{F}$ is the Jacobian matrix of the state transition function, which reflects the locally linear characteristics of the system dynamics, and $\mathbf{Q}$ is the covariance matrix of process noise, which represents the influence of model uncertainty and external disturbances. $\mathbf{H}$ is the Jacobian matrix of the observation function. $\mathbf{R}$ is the covariance matrix of the observation noise, which reflects the uncertainty of the measurement equipment. $\mathbf{z}_k$ and $h(\cdot)$ are the measurement quantity and the measurement function respectively.

### C. Dynamic State Estimation by Unscented Kalman Filter

The UKF adopts a fundamentally different approach from the EKF. Instead of linearizing the nonlinear functions, it directly approximates the probability distribution of the state through a deterministic sampling strategy, which is more suitable for highly nonlinear systems than the EKF.

When implementing the UKF algorithm, the sigma point sampling is first conducted. Based on the current state estimation of $\hat{x}_{k-1}$ and the covariance $\mathbf{P}_{k-1}^+$, a set of $2n+1$ sigma points ($n$ is the state dimension) is generated as follows:

$$\chi_{k-1}^{(i)} = \begin{cases} \hat{\mathbf{x}}_{k-1}, & i = 0 \\ \hat{\mathbf{x}}_{k-1} + \gamma \cdot \sqrt{\mathbf{P}_{k-1}^+}_i, & i = 1, \ldots, n \\ \hat{\mathbf{x}}_{k-1} - \gamma \cdot \sqrt{\mathbf{P}_{k-1}^+}_{i-n}, & i = n+1, \ldots, 2n \end{cases} \tag{10}$$

where $\gamma = \sqrt{n+\lambda}$ is the scaling factor and $\lambda = \alpha^2(n+\kappa) - n$ is the composite parameter. Then, each sigma point is propagated through the nonlinear state equation $f(\cdot)$ to obtain the predicted sigma point set:

$$\chi_k^{(i)} = f\left(\chi_{k-1}^{(i)}, \mathbf{u}_{k-1}\right), \quad i = 0, 1, \ldots, 2n \tag{11}$$

Next, the weighted average of the propagated sigma points is calculated to obtain the predicted state and covariance:

$$\begin{aligned} \hat{\mathbf{x}}_k^- &= \sum_{i=0}^{2n} W_m^{(i)} \chi_k^{(i)} \\ \mathbf{P}_k^- &= \sum_{i=0}^{2n} W_c^{(i)} \left(\chi_k^{(i)} - \hat{\mathbf{x}}_k^-\right)\left(\chi_k^{(i)} - \hat{\mathbf{x}}_k^-\right)^T + \mathbf{Q} \end{aligned} \tag{12}$$

where, $W_m$ and $W_c$ represent the weights of the mean and covariance, respectively. Then, the measurement is updated:

$$\mathcal{Z}_k^{(i)} = h\left(\chi_k^{(i)}\right), \quad i = 0, 1, \ldots, 2n \tag{13}$$

Then, the measurement-predicted mean, covariance, cross-covariance, Kalman gain and the state can be updated:

$$\begin{aligned} \hat{\mathbf{z}}_k^- &= \sum_{i=0}^{2n} W_m^{(i)} \mathcal{Z}_k^{(i)} \\ \mathbf{P}_{zz} &= \sum_{i=0}^{2n} W_c^{(i)} \left(\mathcal{Z}_k^{(i)} - \hat{\mathbf{z}}_k^-\right)\left(\mathcal{Z}_k^{(i)} - \hat{\mathbf{z}}_k^-\right)^T + \mathbf{R} \\ \mathbf{P}_{xz} &= \sum_{i=0}^{2n} W_c^{(i)} \left(\chi_k^{(i)} - \hat{\mathbf{x}}_k^-\right)\left(\mathcal{Z}_k^{(i)} - \hat{\mathbf{z}}_k^-\right)^T \\ \mathbf{K}_k &= \mathbf{P}_{xz}\left(\mathbf{P}_k^-\right)^{-1} \\ \hat{\mathbf{x}}_k^+ &= \hat{\mathbf{x}}_k^- + \mathbf{K}_k\left(\mathbf{z}_k - \hat{\mathbf{z}}_k^-\right) \\ \mathbf{P}_k^+ &= \mathbf{P}_k^- - \mathbf{K}_k\mathbf{P}_k^-\mathbf{K}_k^T \end{aligned} \tag{14}$$

When applying UKF to VSG state estimation, we directly use the state equation $f(\cdot)$ and observation equation $h(\cdot)$ in subsection III-A as the propagation functions for the sigma points, with no need for Jacobian computation (linearization).

## IV. Experiments and Results

To inspect the estimation performance of the two Kalman filtering methods, in this section we present experiments in Simulink for two cases. The simulation time $t_{max}$ is set to 0.5 seconds, and the sampling time interval $\Delta t$ is set to $10^{-4}$ seconds. In Case 1, the VSG is connected to a constant voltage source (mimicking the "infinity bus"). In Case 2, the VSG is connected to a system with 3 machines and 9 buses. The Simulink model of VSG is shown in Fig. 3. The pseudo-code of the experimental process is shown in **Algorithm 1**.

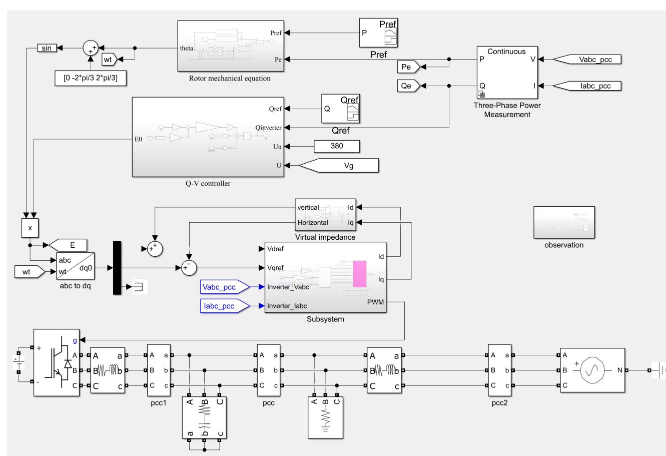


Fig. 3. The Simulink model of the VSG in an infinity-bus system

### A. Simulation Settings

In reality, the internal states of VSG are hard to obtain through measurement. During the experiment, we only use the real-time measured rotor angle and frequency to verify the

979-8-3315-8138-1

**Algorithm 1** Dynamic State Estimation for VSG

**Initialize VSG System Parameters**
$J, k_f, D, \omega_n, X_{total}, V_{grid}, U_B, S_B \leftarrow$ physical parameters
$\theta_0, \omega_0 \leftarrow$ initial states
$\Delta t, t_{max} \leftarrow$ simulation parameters
$\mathbf{P_0}, \mathbf{Q}, \mathbf{R} \leftarrow$ covariance matrices
$\alpha, \beta, \kappa \leftarrow$ UKF parameters
**Simulate VSG System**
Run Simulink model to collect measurements
$[P_{ref}, P_e, U_n, U_{inv}, Q_{ref}, Q_{inv}, \theta_{grid}] \leftarrow$ measurement data
Preprocess and downsample data
**Execute Estimation Algorithms**
if jacobian can be easily computed:
    $\hat{X}_{EKF} \leftarrow$ EKF_Estimation($\mathbf{X_0}, \mathbf{P_0}, \mathbf{Q}, \mathbf{R}, u$)
    $MAE_{EKF} \leftarrow$ CalculateMAE($\hat{X}_{EKF}, X_{true}$)
else:
    $\hat{X}_{UKF} \leftarrow$ UKF_Estimation($\mathbf{X_0}, \mathbf{P_0}, \mathbf{Q}, \mathbf{R}, u$)
    $MAE_{UKF} \leftarrow$ CalculateMAE($\hat{X}_{UKF}, X_{true}$)
Calculate execution time

accuracy of the method, but do *not* use them as the input for the EKF or UKF methods. The inputs for EKF and UKF are all obtained from the non-VSG part of the main circuit.

In Case 2, the WSCC 9-bus system is adopted. During the simulation experiment, we connected the VSG model to one of the load buses through a transformer. The constructed Simulink model of Case 2 is shown in Fig. 4.

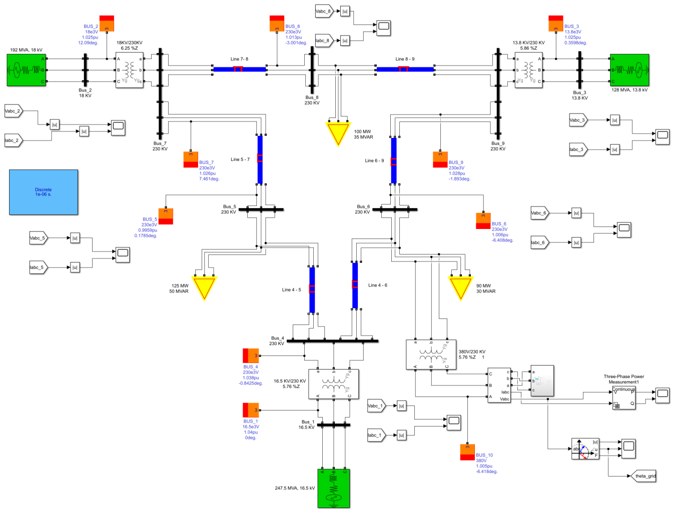

Fig. 4. The Simulink model of the VSG in a 3-machine 9-bus system

Since the resolution of the simulation data is high and uneven, it is necessary to uniformly down-sample the data for EKF and UKF's inputs, as well as for the measured actual values of the VSG "rotor" angle and frequency.

Then, EKF and UKF are run separately in the two cases. The MAE and the time consumption of the two algorithms in the two cases are respectively recorded and compared.

### B. EKF and UKF for VSG Dynamic State Estimation

To make the results more intuitive, from now on we will use the relationship $f = \omega/2\pi$ to convert the angular frequency $\omega$ into frequency $f$. Fig. 5 to 6 show the tracking performance of the two different filtering methods within a 0.5-second window under the two cases. The blue solid line means the actual values obtained via simulation, while the red dashed line means the estimated value by the Kalman filtering method(s). It can be seen that the red line closely follows the blue line, indicating that both filtering methods accurately tracked the changes in the VSG rotor angle and frequency.

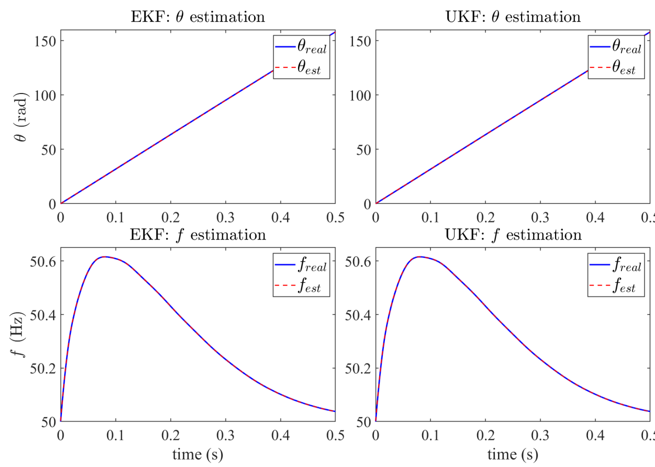


Fig. 5. The estimation results of Case 1 in the steady state

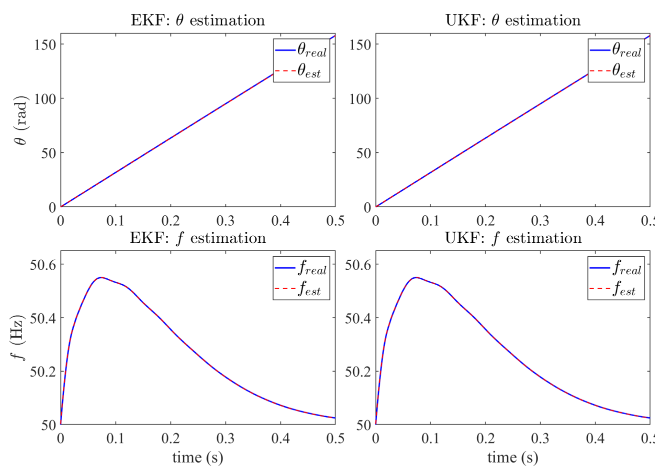


Fig. 6. The estimation results of Case 2 in the steady state

The MAE between the estimated and actual values of the rotor angle and frequency are calculated, as shown in Table I.

It can be seen that in Case 1, the MAE of the rotor angle estimation by EKF is basically the same as that by UKF, approximately $0.141$ rad. The MAE of the frequency estimation using EKF is $2.473 \times 10^{-4}$ Hz, which is lower than $3.153 \times 10^{-4}$ Hz obtained using UKF. Similarly, in Case 2, the MAE of the rotor angle estimation by EKF and UKF

979-8-3315-8138-1

TABLE I
THE MAE OF ROTOR ANGLE AND FREQUENCY ESTIMATION

| **Case** | **Method** | **MAE** | | **Time (s)** |
|---|---|---|---|---|
| | | $\theta$ **(rad)** | $f$ $(10^{-4}$**Hz)** | |
| Case 1 | EKF | 0.141 | 2.473 | 0.132 |
| Case 1 | UKF | 0.141 | 3.153 | 0.375 |
| Case 2 | EKF | 0.131 | 2.236 | 0.107 |
| Case 2 | UKF | 0.131 | 2.699 | 0.296 |

is approximately 0.131 rad, while the MAE of the frequency estimation by EKF is $2.236 \times 10^{-4}$Hz, which is lower than $2.699 \times 10^{-4}$ Hz obtained by UKF.

It can be observed that in both cases, the estimation of EKF is superior to that of UKF. This might be because UKF is more suitable for highly nonlinear systems, while EKF can achieve good results with a first-order approximation when the nonlinearity is not severe. Here, the VSG model is second-order, so its degree of nonlinearity is moderate. Therefore, using EKF can achieve high enough accuracy.

The time costs of the two algorithms in the two cases are shown in Table I. It can be seen that in either the single-machine infinity-bus system or the three-machine nine-bus system, EKF runs faster than UKF. This is because UKF needs to perform propagation operations on a large number of samples. When using EKF, after computing the Jacobian matrix, the prediction and update steps degenerate into a standard linear Kalman filtering form. Therefore, in both cases, EKF performs more efficiently than UKF.

Furthermore, in order to study the estimation performance of EKF and UKF under the non-steady state conditions of the power system, we add frequency variations of the voltage source to the single-machine system and add load variations to the nine-bus system. The performances of the two algorithms after adding those disturbances are shown in Table II, and depicted in Fig. 7 and 8, with similar conclusions being drawn.

TABLE II
THE MAE OF ROTOR ANGLE AND FREQUENCY ESTIMATION UNDER DISTURBED CONDITION

| **Case** | **Method** | **MAE** | | **Time (s)** |
|---|---|---|---|---|
| | | $\theta$ **(rad)** | $f$ $(10^{-4}$**Hz)** | |
| Case 1 | EKF | 0.205 | 0.089 | 0.103 |
| Case 1 | UKF | 0.205 | 1.413 | 0.357 |
| Case 2 | EKF | 0.101 | 1.175 | 0.095 |
| Case 2 | UKF | 0.101 | 2.597 | 0.316 |

## V. CONCLUSION

This study compares the performance of EKF and UKF in the dynamic state estimation task for VSG. The main conclusion is that in the two cases studied, EKF performed better in an overall sense in both accuracy and speed.

In systems with higher-order dynamics under more severe nonlinearities, the performance of UKF may be more competitive. Future work includes: 1) evaluate the filter for more

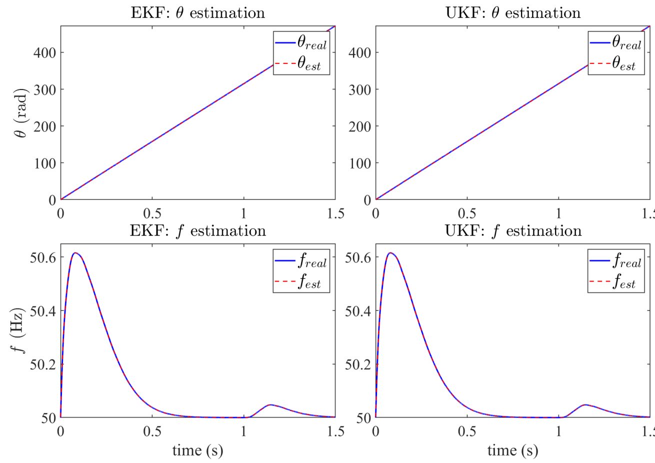


Fig. 7. The estimation results of Case 1 after adding source disturbance

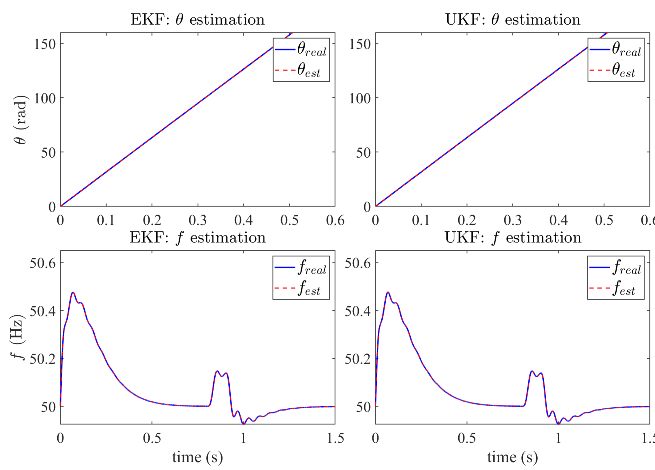


Fig. 8. The estimation results of Case 2 after adding load disturbance

detailed VSG models; 2) test the algorithms under more severe grid disturbances to assess their robustness; 3) explore more filtering methods that may have higher efficiency or accuracy.

## REFERENCES

[1] Zhao J, Mili L, Gómez-Expósito A. "Constrained robust unscented Kalman filter for generalized dynamic state estimation", *IEEE Transactions on Power Systems*, 2019, 34(5): 3637-3646.
[2] Kotha S K, Rajpathak B, Mallareddy M, et al. "Dynamic state estimation of power system using hybrid whale-tunicate optimized unscented Kalman filter based on wide area measurement systems", *Electric Power Systems Research*, 2024, 230: 110242.
[3] Wang Y, Wang Y, Sun Y, et al. "Resilient dynamic state estimation for multi-machine power system with partial missing measurements", *IEEE Transactions on Power Systems*, 2023, 39(2): 3299-3309.
[4] Zhang X, Gong L, Zhao X, et al. "Voltage and frequency stabilization control strategy of virtual synchronous generator based on small signal model", *Energy Reports*, 2023, 9: 583-590.
[5] Zhang J, Wang H, Liu G, et al. "Virtual synchronous generator control strategy of grid-forming matrix converter for renewable power generation", *IEEE Access*, 2024.
[6] Tahir W, Farhan M, Bhatti A R, et al. "A modified control strategy for seamless switching of virtual synchronous generator-based inverter using frequency, phase, and voltage regulation", *International Journal of Electrical Power & Energy Systems*, 2024, 157: 109805.

979-8-3315-8138-1